Int. J. Electrochem. Sci., 4 **(2009)** 755 - 761

International Journal of
ELECTROCHEMICAL
SCIENCE
www.electrochemsci.org

Formation and Lithiation of Ferroselite Nanoflowers as High-energy Li-ion Battery Electrodes

L.Q. Mai[1,2,*], *Y. Gao*[1], *J.G. Guan*[1], *B. Hu*[1], *L. Xu*[1], *W. Jin*[1]

[1] State Key Laboratory of Advanced Technology for Materials Synthesis and Processing, School of Materials Science and Engineering Wuhan University of Technology, Wuhan, 430070, China
[2] Department of Chemistry and Chemical Biology, Harvard University, Cambridge, Massachusetts 02138, USA
[*]E-mail: mlq@cmliris.harvard.edu

Received: 3 May 2009 / *Accepted:* 20 May 2009 / *Published:* 6 June 2009

Ferroselite ($FeSe_2$) nanoflowers were prepared by a mild hydrothermal method at 170°C with Na_2SeSO_3 and FeC_2O_4 as the raw materials, and lithiated through a secondary hydrothermal reaction with Li salt solution. The products were characterized by XRD, FE-SEM, EDS, CV and model battery testing. The results show that the as-prepared $FeSe_2$ nanoflowers composed of uniform nanoplates about 20 nm in thickness and 100 nm in diameter, exhibit high discharge capacity of ca. 431 mAh/g. Notably, the capacity retention rate of $FeSe_2$ nanoflower electrodes is greatly improved from 45% before lithiation to 63% after lithiation through secondary hydrothermal lithiation modification and this improvement of cycling property is confirmed by CV investigation, probably resulting from increase of structure stability and weakening of electrostatic interaction between $FeSe_x$ layers and Li^+ ions in interlayer during the discharge when Li ions occupy the interstitial site of $FeSe_2$ lattice.

Keywords: Ferroselite nanoflowers, Lithiation, Secondary hydrothermal reaction, Electrochemistry

1. INTRODUCTION

Considerable attention has been devoted to complex nanostructures with different morphology, orientation, and dimensionality due to their size- and shape-dependent photocatalytical, optical, electrical, photoelectric properties [1-3]. Wurtzite ZnSe hierarchical nanostructures with high photocatalytic activity have been synthesized and the flowerlike morphology is important for the excellent photocatalytic activity [3]. Meanwhile, in development of energy storage devices, nanostructured electrode materials have attracted great interest in the field of lithium-ion batteries, essentially because of their substantial advantages, such as short transport path lengths for electrons and Li^+ ions, a large amount of contact surface area between the electrode and electrolyte, and large

flexibility and toughness for accommodating strain introduced by Li^+ insertion/extraction [4, 5]. Among the researches on Li ion battery cathode materials, there is a strong desire to find alternatives to cobalt-based oxides used in commercial batteries because of their high cost, toxicity and limited capacity. It is also challenging to overcome the issues associated with fast capacity fading and poor stability involving large structure and volume changes during Li^+ ion insertion and extraction, poor electron and ion conduction.

Recently ferroselite ($FeSe_2$) has been investigated as a VIII-VI semiconductor with a direct 1.0 eV band gap [6] and as a model system to explore chemical processes and applications in electronics, optics, optoelectronics, and for spintronic devices [7-9]. To date, some efforts have been made to prepare transition metal diselenides nanocrystallites through solution-phase route. For example, MSe_2 (M=Ni, Co, Fe) were prepared by a solvothermal-reduction process [10] or through a hydrothermal co-reduction route [11]. Moreover, Fe-based compounds are more advantageous as electrode materials for lithium ion batteries because iron is abundant, cheap and environmentally friendly [12, 13]. However, until now, there are few reports on synthesis of $FeSe_2$ nanoflowers, and Li^+ ion insertion and extraction behavior and electrochemical properties for this novel nanomaterial are very poorly understood, which limits their wide application in energy field. In the present work, we report hydrothermal preparation and secondary hydrothermal lithiation of $FeSe_2$ nanoflowers, which show that $FeSe_2$ nanoflowers represent an attractive alternative for Li ion batteries based on the considerable enhancement in specific capacity and cycling property and potential advantages from an environmental point of view.

2. EXPERIMENTAL PART

A. Synthesis and lithiation of $FeSe_2$ nanoflowers. Sodium selenosulfate (Na_2SeSO_3) and 9.1 wt% PVA sol were prepared according to the literature [14, 15]. In a typical reaction, 2.5mmol of ferrous oxalate FeC_2O_4 was dissolved in 5ml of 1M citric acid under magnetic stirring to form a homogeneous solution. Then a certain amount of ammonia, 25 ml of 0.1M sodium selenosulfate solution and 25ml of 9.1wt% PVA sol were introduced into the former solution to form the final solution (pH =9) with constantly vigorous stirring. The resulting solution was transferred into a Teflon-lined autoclave of 100mL capacity, which was then sealed and maintained at 180 °C for 24h, then naturally cooled to room temperature in air. The resulting dark red precipitates were centrifuged and washed with absolute ethanol and 0.2M HCl for several times. Then the products were dried at 60 ^oC under vacuum for 6 h, and the $FeSe_2$ nanoflowers obtained. To attain the lithiated $FeSe_2$ nanoflowers, 0.20 g $FeSe_2$ nanoflowers were dispersed by ultrasonic treatment in deionized water for half an hour. Subsequently the dispersed $FeSe_2$ nanoflowers were stirred with 0.29 g LiCl for 2 days, and the resultant light-blue solution was transferred into a 100 mL Teflon-lined autoclave. The autoclave was sealed and heated at 180 °C for 24 h. Next, the autoclave was left to cool down in air and the solid precipitate was filtered out and washed with deionized water at least five times to remove the LiCl adsorbed on the surface of the nanoflowers.

B. Characterization of the products. X-ray diffraction (XRD) measurement was performed using a D/MAX-III X-ray diffractrometer. The morphologies of the as-prepared samples were

observed by a Hitachi S-4800 field-emission scanning electron microscope (FE-SEM) equipped with an X-ray energy dispersive spectrometer (EDS), at an acceleration voltage of 20 kV. The electrochemical properties were studied with a multichannel battery testing system. Batteries were fabricated using a lithium pellet as the negative electrode; 1M solution of $LiPF_6$ in ethylene carbon (EC)/dimethyl carbonate (DMC) as the electrolyte; and a pellet made of the nanoflowers, acetylene black and PTFE in a 10:7:1 ratio as the positive electrode. Cell charge and discharge cycling was studied at a current density of 40 mA/g with the cut-off potentials being 1.05–3.0 V vs. Li/Li^+. The cyclic voltammograms (CV) were measured at the scan rate of 0.2 mV/s with an Autolab model PGSTAT30 (GPES/FRA) potentiostat/galvanostat interfaced to a computer.

3. RESULTS AND DISCUSSION

Fig. 1 shows the XRD pattern of the $FeSe_2$ nanoflowers. All the diffraction peaks in the Fig. 1 can be readily indexed on the basis of an orthorhombic cell with crystallographic parameters a = 4.8002 Å, b=5.7823 Å, and c = 3.5834 Å (JCPD No. 82-0269) corresponding with that of the bulk $FeSe_2$. No peaks of other crystalline phases are detected in the XRD pattern, indicating that a pure $FeSe_2$ phase has been attained.

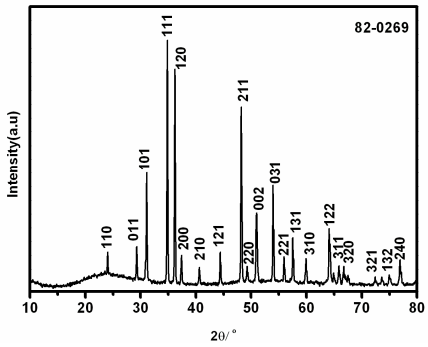

Figure 1. XRD pattern of the as-prepared products.

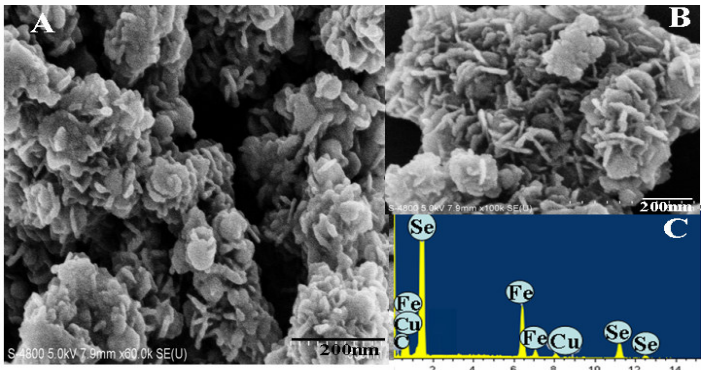

Figure 2. Typical FE-SEM images (A, B) and EDS spectrum (C) of the as-prepared $FeSe_2$ nanoflowers.

Fig. 2 shows the FE-SEM images and EDS spectrum of the as-prepared $FeSe_2$ nanoflowers by this one-step solution approach. The FE-SEM images of the nanoflowers at different locations and magnifications reveal that the $FeSe_2$ nanoflowers are composed of uniform nanoplates about 20 nm in thickness and 100 nm in diameter. EDS investigation (Figure 2C) indicates the presence of Fe and Se elements, and the Cu and C peaks may originate from the sample grid.

Fig. 3A shows the curves of discharge capacity versus the cycle number for the $FeSe_2$ nanoflowers before and after lithiation at a current density of 40 mA/g and at a temperature of 25 °C. For the nonlithiated $FeSe_2$ nanoflowers, the first discharge and the second discharge capacities reach 431 mAh/g and 382 mAh/g, respectively, with a large irreversible capacity of about 49 mAh/g in the first cycle. The irreversible capacity is supposed to result from the reaction of Li with electrolyte to form a layer of passivating film on the surface of the electrode due to the surface effect of the $FeSe_2$ nanostructures and the solid electrolyte interface (SEI) formation reactions on the surface of $FeSe_2$ electrode [16,17]. For the lithiated $FeSe_2$ nanoflowers, a smaller irreversible capacity of about 36 mAh/g in the first cycle is observed. After 25 cycles, the discharge capacity of the nonlithiated $FeSe_2$ nanoflowers decreases to 192 mAh/g, corresponding to a capacity retention of 45%. However, for the lithiated $FeSe_2$ nanoflowers, the discharge capacity decreases to 242 mAh/g after 25 cycles, corresponding to a capacity retention of 63% and showing the enhancement of cycling performance of the lithiated nanoflowers. Fig. 3B shows the potential versus capacity curve of the second cycles for the nonlithiated and lithiated $FeSe_2$ nanoflowers. Two plateaus are evident in the second discharge process for nonlithiated and lithiated $FeSe_2$ nanoflowers, suggesting that the lithium insertion proceeds in two steps with the first capacity ranges of 48–115 mAh/g at about 2.0 V and the second 200–330 mAh/g at about 1.50 V. We note that the lithiated $FeSe_2$ nanoflowers exhibit a lower discharge capacity than that of the non-lithiated $FeSe_2$ nanoflowers, which may be because some Li^+ ions introduced during the secondary hydrothermal lithiation process have occupied some space of the interstitial sites that are electrochemically active for Li^+-storage [18,19]. The pre-intercalation of Li^+ ions into $FeSe_2$ nanoflowers significantly enhances the cycling stability and reversibility, and the Li^+ ions which occupy the interstitial site of $FeSe_2$ lattice stabilize the structure and reduce the electrostatic interaction between $FeSe_x$ layers and Li^+ ions in interlayer during the discharge.

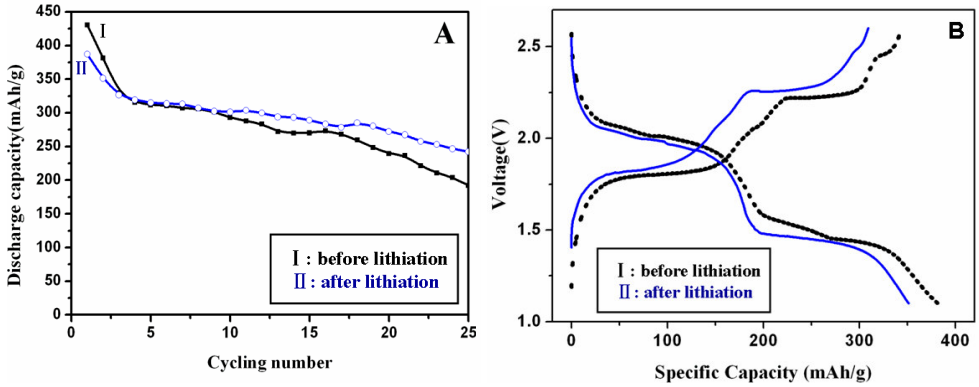

Figure 3. (A) The discharge capacity as a function of the cycle number for the $FeSe_2$ nanoflowers before and after lithiation. (B) Potential vs. capacity curves for the second cycle of charge-discharge process of the nanoflowers before and after lithiation.

The cycling behavior can be modeled using a relation giving the capacity as a function of the cycle number, the fraction loss is calculated by the following equation:

$$C_n = C_0(1-\delta)^n$$

where C_0 = the initial capacity
n = the cycle number
δ = the fraction loss per cycle

The twenty-fifth fraction loss δ_{25} of the lithiated $FeSe_2$ nanoflowers is 1.86%, which is lower than that of nonlithiated $FeSe_2$ nanoflowers (3.17%). The lower fraction loss of the lithiated $FeSe_2$ nanoflowers indicates they exhibit much less capacity loss per cycle. Owing to its high reversible capacity and good cycling stability in the following cycles, the lithiated $FeSe_2$ nanoflowers are demonstrated to be a promising cathode material for future rechargeable lithium batteries.

Fig. 4A and 4B show the cyclic voltammograms of the nonlithiated and lithiated $FeSe_2$ nanoflowers, respectively, in which the first, second, fifth and tenth cycle curves are plotted. There are two sets of (cathodic, anodic) current peaks appearing at around the potential (V) of (1.56, 2.01) and (1.22, 2.50) in the first cycle curve of the nonlithiated $FeSe_2$ nanoflowers (Fig. 4A), and the first set of peaks shift to the potential (V) of (1.69, 2.09) in the next cycles. There are some oxide-layer on the surface of the $FeSe_2$ nanoflowers can induce the different current peaks among the first and the following cycles. These two sets of peaks can be assigned to the insertion/extraction of Li^+ ions between the orthorhombic $FeSe_2$ nanoflowers, respectively, and the proposed processes for the insertion/extraction of Li^+ ions can be described as follows:

$$FeSe_2 + Li^+ + e^- \rightarrow FeLiSe_2$$

$$FeSe_2 + 2Li^+ + 2e^- \rightarrow Li_2Se_2 + Fe$$

As shown in Fig. 4B, there are two sets of (cathodic, anodic) current peaks appearing at around the potential (V) of (1.81, 2.01) and (1.33, 2.40) in the fifth and the tenth cycle curve of the lithiated $FeSe_2$ nanoflowers. Obviously, the anodic peaks of the lithiated $FeSe_2$ nanoflowers located at 2.01 and 2.40 V are more intensive than that of the nonlithiated $FeSe_2$ nanoflowers, indicating more Li^+ ions are extracted from the lithiated $FeSe_2$ lattice. Compared to the nonlithiated $FeSe_2$ nanoflowers, the cathodic and anodic current peaks located at 2.40V and 1.33V are much more intensive, which indicates that the reversibility of Li^+ ions insertion/extraction between the lithiated $FeSe_2$ nanoflowers is better than that of the nonlithiated $FeSe_2$ nanoflowers. Meanwhile, the fifth and tenth cycle curves of the lithiated $FeSe_2$ nanoflowers almost coincide with each other in Fig. 4B, showing that the structure of the lithiated $FeSe_2$ nanoflowers is very stable after five cycles, and the lithiated $FeSe_2$ nanoflowers electrode is suffered from structure adjusting at the first five charge/diacharge cycles. It is well-known that the area surrounded by each cycle curve represents the amount of the Li^+ ions insertion, so the capacity of the lithiated $FeSe_2$ nanoflowers is higher than that of nonlithiated after the first 10

charge/diacharge cycles, and this result is in good agreement with that obtained by above cycling property test. All these results indicate that lithiated $FeSe_2$ nanoflowers are promising cathode materials in lithium ion batteries.

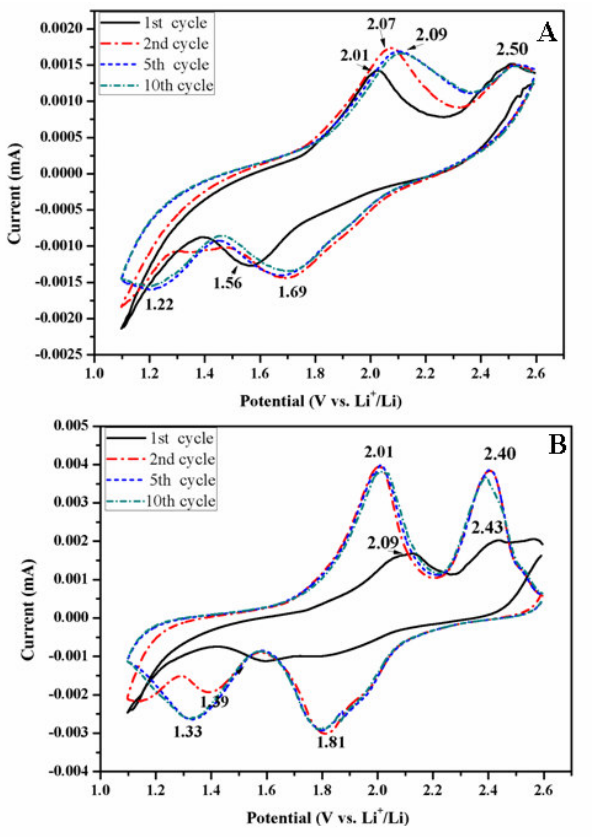

Figure 4. Cyclic voltammograms of the $FeSe_2$ nanoflowers before (A) and after lithiation (B) in the first, second, fifth and tenth cycles.

4. CONCLUSIONS

$FeSe_2$ nanoflowers composed of uniform nanoplates about 20 nm in thickness and 100 nm in diameter were successfully synthesized via a facile hydrothermal method, and lithiation modification of $FeSe_2$ nanoflowers was conducted by a secondary hydrothermal method. Battery test shows that the reversible capacity of $FeSe_2$ in the first cycle reaches 431 mAh/g, and capacity retention rate is 45% after 25 cycles, while the discharge capacity of the lithiated $FeSe_2$ nanoflowers still maintains 242 mAh/g after 25 cycles, with a capacity retention rate of 62.6%. The cyclic voltammograms of the pristine and lithiated $FeSe_2$ nanoflowers, also show the lithiated $FeSe_2$ nanoflowers exhibit good cycling capability and it is suitable for use as high-property electrode material in rechargeable lithium-ion batteries.

ACKNOWLEDGEMENTS
This work was supported by the National Nature Science Foundation of China (50702039), the Research Fund for the Doctoral Program of Higher Education (20070497012), Scientific Research Foundation for Returned Scholars, Ministry of Education of China (2008-890) and Innovation Special Foundation of Excellent Returned Scholars of Wuhan (2008-84). The authors are pleased to thank the strong support and helpful discussion of Prof W Chen of Wuhan University of Technology.

References

1. B. Z. Tian, X. L. Zheng, T. J. Kempa, Y. Fang, N. F. Yu, G. H. Yu, J. L. Huang, C. M. Lieber, *Nature*, 449(2007)885-889.
2. L. Q. Mai, Y. H. Gu, C. H. Han, B. Hu, W. Chen, P. C. Zhang, L. Xu, W. L. Guo, Y. Dai, *Nano. Lett.* , 9 (2009) 826.
3. F. Cao, W. D. Shi, L. J. Zhao, S. Y. Song, J.H. Yang, Y. Q. Lei, H. J. Zhang, *J. Phys. Chem. C,* 112 (2008) 17095.
4. L. Q. Mai, B. Hu, Y. Y. Qi, Y. Dai, W. Chen, *Int. J. Electrochem. Sci.,* 3 (2008) 216.
5. Y. S. Hu, L. Kienle, Y. G. Guo, J. Maier, *Adv. Mater.,* 18 (2006) 1421.
6. T. Harada, *J. Phys. Soc. Jpn.,* 67 (1998) 1352.
7. M. Bruchez, M. Moronne, P. Gin, S. Weiss, A. P. Alivisatos, *Science,* 281 (1998) 2013.
8. C. Ma, Y. Ding, D. Moore, X. Wang, Z. L. Wang, *J. Am. Chem. Soc.,* 126 (2004) 708.
9. Z. W. Wang, L. L. Daemen, Y. S. Zhao, C. S. Zha, R. T. Downs, X. Wang, Z. L. Wang, R. J. Hemley, *Nat. Mater.,* 126 (2004) 708.
10. Y. Xie, L.Y. Zhu, X. C. Jiang, J. Lu, X. W. Zheng, W. He, Y. Z. Li, *Chem. Mater.,* 13 (2001) 3927.
11. A. P. Liu, X. Y. Chen, Z. J. Zhang, Y. Jiang, C. W. Shi, *Solid State Commun.,* 138 (2006) 538.
12. J. M. Yan, H. Z. Huang, J. Zhang, Z. J. Liu, Y. Yang, *J. Power sources,* 146 (2005) 264.
13. R. Z. Yang, Z. X. Wang, J. Y. Liu, L. Q. Chen, *Electrochem. Solid-Satate Lett.,* (2004) 7, A496.
14. B. Pejova, M. Najdoski, I. Grozdanov, S. K. Dey, *Mater. Lett.,* 43 (2000) 269.
15. Q. Xie, Z. P. Liu, M. W. Shao, L. F. Kong, W. C. Yu, Y. T. Qian. *J. Cryst. Growth,* 252 (2003) 570.
16. D. Aurbach, M. D. Levi, E. Levi, A. Schechter, *J. Phys. Chem., B* 101 (1997) 2195.
17. J. Xie, X. B. Zhao, G. S. Cao, M. J. Zhao, Y. D. Zhong, L. Z. Deng, *Mater. Lett.* 57 (2003) 4673.
18. L. Q. Mai, B. Hu, W. Chen, Y. Y. Qi, C. S. Lao, R. S. Yang, Y. Dai, Z. L. Wang, *Adv. Mater.* 19 (2007) 3712.
19. Y. Y. Qi, W. Chen, L. Q. Mai, Q. R. Zhu, A. P. Jin, *Int. J. Electrochem. Sci.,* 1 (2006) 317.